nature communications

Article

https://doi.org/10.1038/s41467-024-53049-z

Universal high-efficiency electrocatalytic olefin epoxidation via a surface-confined radical promotion

Received: 22 February 2024

Accepted: 27 September 2024

Published online: 15 October 2024

Check for updates

Pan Ran[1,2], Aoqian Qiu[1,2], Tianshu Liu[1], Fangyuan Wang[1], Bailin Tian[1], Beiyao Xiang[1], Jun Li[1], Yang Lv[1] & Mengning Ding[1]

Production of epoxides via selective oxidation of olefins affords a fundamental source of key intermediates for the industrial manufacture of diverse chemical stocks and materials. Current oxidation strategy generally works under harsh conditions including high temperature, high pressure, and/or request for potentially hazardous oxidants, leading to substantial challenges in sustainability and energy efficiency. To this end, direct electrocatalytic epoxidation poses as a promising solution to these issues, yet their industrial applications are limited by the low selectivity, low yield, and poor stability of the electrocatalysts. Here we report a universal electrochemical epoxidation approach via a kinetically confined surface radical pathway. High epoxidation efficiency can be achieved under mild working conditions (e.g., >99% selectivity, >80% yield and >80% Faraday efficiency for cyclohexene-to-cyclohexene oxide conversion), which can be extended to broad scope of olefin substrates. The catalytic performance originated from a surface bimolecular (L-H) reaction mechanism involving formation and surface confinement of bromine radicals due to kinetic restriction, which effectively activates inert C=C bonds while avoiding the homogenous radical side reactions. With the use of renewable energy and water as green oxygen source, successful implementation of this approach will pave the way for more sustainable chemical production and manufacturing.

Epoxy compounds are essential raw materials widely used for the synthesis of a broad range of commercial products, including solvents, resins, plastics, and coatings[1,2]. For instance, several key epoxy compounds, including ethylene, propylene, cyclohexane, and styrene oxides, are extensively employed as precursors for various surfactants, insecticides, epoxy resins, pharmaceuticals, and fragrances[3–6]. As a result, the olefin epoxidation process is considered a key foundation in the chemical, petroleum, and materials industries. However, current epoxy compounds are manufactured via chlorohydrin route[5,7] and aerobic/peroxide oxidation via heterogeneous catalysis[8–10], which often require harsh conditions, and suffer from high energy consumption, high cost, and/or potential hazards/risks[11–13]. More importantly, these strategies were ultimately powered by the consumption of fossil fuels, leading to a significant carbon footprint. Another critical issue is that the majority of state-of-the-art oxidation methods are effective only for a limited range of alkene substances. For example, thermo-catalytic epoxidation of olefins using O_2 or H_2O_2 shows poor efficiencies when applied to cyclic and straight-chain olefins[14–18], whereas the chlorohydrin-based methodologies have been demonstrated effective only for conjugated olefins (Fig. 1a)[19]. There is no doubt an urgent need for a more efficient strategy driven by renewable energy to meet the production requirements in sustainability and chemical compatibility.

[1]Key Laboratory of Mesoscopic Chemistry, School of Chemistry and Chemical Engineering, Nanjing University, Nanjing, Jiangsu, China. [2]These authors contributed equally: Pan Ran, Aoqian Qiu. e-mail: mding@nju.edu.cn

https://doi.org/10.1038/s41467-024-53049-z

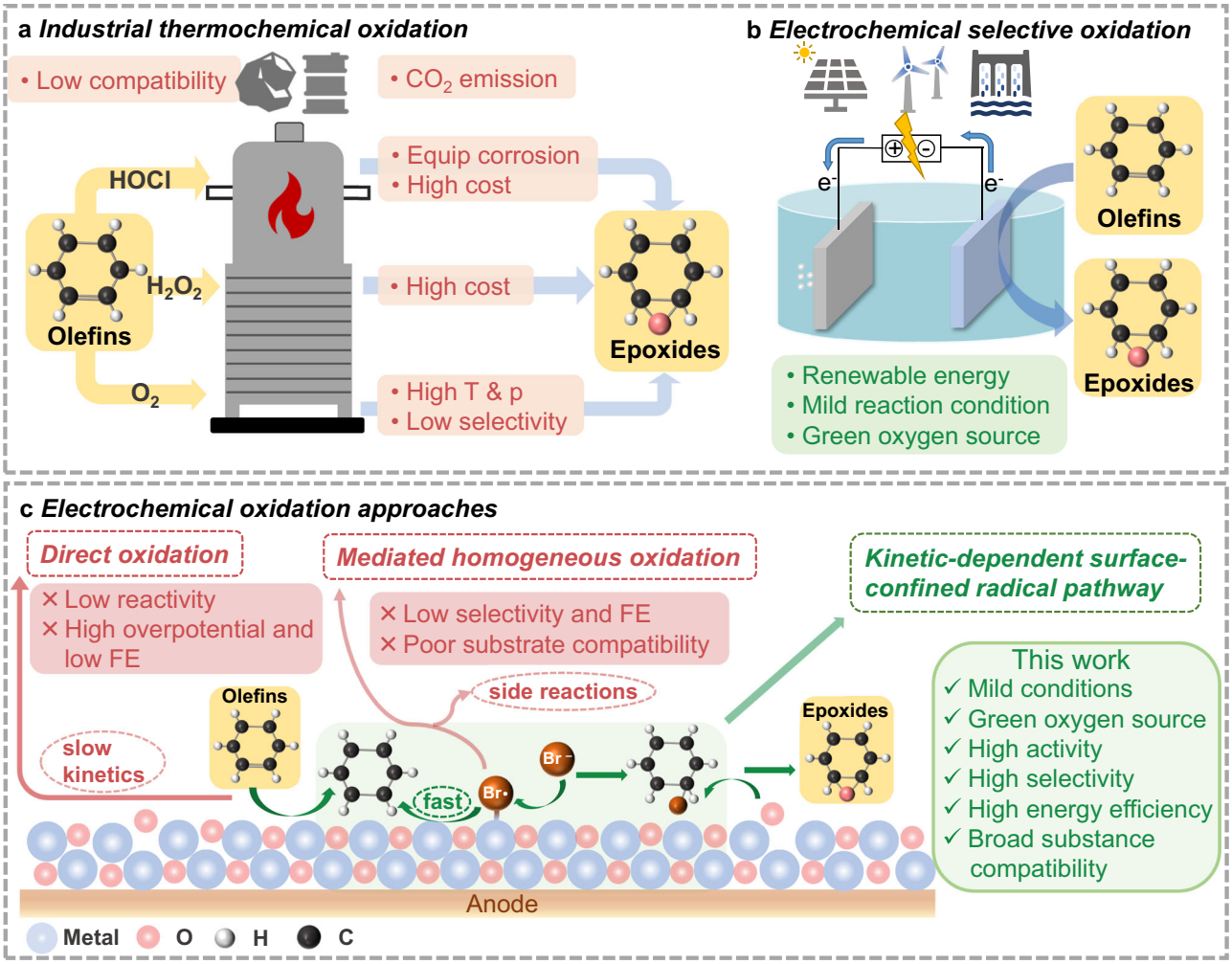

Fig. 1 | Schematic illustration of different strategies for olefin epoxidation. **a**, **b** Comparison of (**a**) industrial thermo-catalytic oxidation methods and (**b**) electrocatalytic oxidation methods. **c** Schematic illustration of the kinetic-dependent surface-confined radical pathway for the efficient electrocatalytic olefin epoxidations, and comparison with direct oxidation and mediator-assisted homogeneous oxidation.

Electrochemical-based selective oxidation produces desired chemical substances by using renewable electricity, thus representing a compelling alternative to the traditional olefin epoxidation approaches (Fig. 1b)[13,20,21]. Its unique advances include mild reaction conditions, excellent energy efficiencies, and the use of water as a green oxygen source[10,21–23]. Direct electro-oxidative epoxidation of cyclooctene was systematically investigated on manganese dioxide[24,25] and ruthenium oxide[26], whereas electrochemical conversion of cyclooctene to cyclooctene oxide was observed on the Au surface[27]. However, the direct electro-oxidation of aliphatic alkenes (such as cyclohexene) poses significant challenges due to their inert C=C bonds and poor adsorption on the electrode surface (Supplementary Fig. S1a), leading to ultrahigh overpotential, inferior conversion, selectivity, and Faraday efficiency[24,25,28–30]. Redox mediators have been developed to activate the C=C bonds. Efficient epoxidation of ethylene was demonstrated using a redox-mediated pathway through hypochlorite generated on the $NiCo_2O_4$[31] and RuO_2[32] and IrO_2/Ti electrode[13,21], and benzoic acid was used as a mediator to assist cycloolefin epoxidation[33]. In addition, photo-excitation was likewise exploited to generate redox-mediating species (such as hypobromite) for olefin epoxidation in photoelectrochemical (PEC) cells[19,34–36]. However, while redox-mediators worked well for the gaseous ethylene, propylene, or conjugated olefins[13,21,36–38], the issue of low current density and poor selectivity remains for the liquid phase epoxidation of non-activated olefins, which accounts for the majority of olefine molecules. Moreover, as a homogeneous process, side reactions easily occur between the mediator and undesired species, which sets a limit to its selectivity substance compatibility. Similar reasons prevent the further application of more reactive mediating species (such as radicals) for better activation without creating uncontrolled side reactions (Supplementary Fig. S1b)[19,35]. Therefore, a surface-confined activation strategy might be a solution to reconfigure the reaction pathway for universally efficient electro-epoxidation of olefin with ideal performance.

Here, we report an electrocatalytic olefin epoxidation approach demonstrating performance toward a remarkably broad scope of olefine substance, via a kinetically confined surface radical pathway. As illustrated in Fig. 1c and Supplementary Fig. S1c, the activation of the C=C bonds is effectively promoted by bromine radicals in situ formed on the electrode. To tackle the general issue of radical-based side reactions during a homogeneous process, the concurrent use of palladium oxide (PdO) catalyst favoring olefin surface adsorption leads to a kinetic restriction on the radical diffusion into solution phase, which results in a bi-molecular surface reaction pathway. The activated olefin intermediates on the surface are consequently attacked by the active surface (lattice) oxygen species from partial water oxidation, to finally afford epoxide products. For the model reaction of cyclohexene-to-cyclohexene oxide conversion, a reduced overpotential by 550 mV was achieved, with yield Faraday efficiency both exceeding 80% and product selectivity of > 99%. These performances surpass the state-of-the-art electrochemical cyclohexene epoxidation methodologies.

Additionally, the same electrocatalytic strategy appears effective for a variety type of olefins, including chain olefins (~70% yield), cyclic olefins (~80% yield), and conjugated olefins (~80% yield). Overall, the successful implementation of this universal epoxidation of olefins, using electricity as the renewable energy source and water as the green oxygen source, paved the way for safer, more sustainable, and more economical chemical/material manufacturing.

Results

Design principles for efficient electrocatalytic epoxidation

As the adsorption of hydrocarbon molecules is generally weak due to the absence of a chemically active group, identification of a catalyst with strong adsorption towards olefines is deemed imperative for efficient modulation of their epoxidation. To this end, PdO was selected as a model catalyst platform due to its potential capability for adequate olefine adsorption[39–42]. Specifically, the PdO samples were prepared using a multi-step fade calcination technique on Pd/C precursors, and a detailed method can be found in **Methods**. The powder X-ray diffraction (XRD) results exhibit characteristic diffraction peaks of tetragonal PdO (Supplementary Fig. S2). Transmission Electron Microscopy (TEM) images demonstrate a nanocrystalline morphology of as-prepared PdO with a size of approximately 6 ± 2 nm (Supplementary Fig. S3), while selected area electron diffraction (SAED) further reveals the lattice stripes with a crystallographic spacing of 0.210 nm, matching to the (101) plane of PdO. The morphology of the working electrode (carbon paper loaded with PdO) was further investigated by scanning electron microscopy (SEM), and the mapping results reveal the presence of well-dispersed Pd and O elements (Supplementary Fig. S4). As a comparison, the XRD, TEM, and SEM characterization results on the Pd/C electrode can also be found in Supplementary Figs. S3, S4 demonstrating uniformly distributed Pd nanoparticles with a size of approximately 4.5 ± 1 nm. The X-ray photoelectron spectroscopy (XPS) shows a characteristic Pd^{2+} valence state in the metal oxides (Supplementary Fig. S5). Raman spectroscopy (Supplementary Fig. S6) further reveals characteristic vibrational peaks of Pd-O bond[43].

Due to the intrinsic chemical inertness of the C=C double bonds, their activation is challenging yet key to achieving the high-efficiency conversion of olefin molecules after surface adsorption, which presumably requires the coupling of otherwise assisted activation. To this end, the activating agent should possess a potent affinity toward olefin molecules while subject to facile replacement by the consequent oxygen attack, and ideally assume a catalytic, non-sacrificial role during the turnover processes[44–46]. On the basis of these principles, we have first conducted an initial screening on the PdO electrode of several highly active substances commonly used in homogeneous catalysis[45,47–50]. The results depicted in Fig. 2a and Supplementary Fig. S7 indicate that the Bromide ions could efficiently activate the cyclohexene and assist its epoxidation to give the highest yield of cyclohexene oxide. Therefore, tetramethylammonium bromide (TMABr) was employed as both the electrolyte and the activating bromine source in the subsequent investigations, which also avoids the use of extra additives in the general electrolysis set-ups and eliminates the cost of subsequent separation and purification.

Electrocatalytic performance of olefin epoxidation

For the model reaction of cyclohexene epoxidation, linear sweep voltammetry (LSV) and electrochemical impedance spectroscopy (EIS) were first utilized to systematically evaluate the performance of Pd and PdO on the oxidation of water, bromide ions, and cyclohexene oxidation, and the results are shown in Fig. 2b and Supplementary Figs. S8, S9. The oxidation current on the PdO surface exhibited low levels (< 5 mA·cm^{-2}) in the absence of bromide ions. Notably, upon the addition of bromide, a significant surge in the anodic current can be observed on PdO or Pd, accompanied by a substantial decline in the onset potential to 1.35 V vs RHE (V_{RHE}). The electrocatalytic cyclohexene epoxidation performance of PdO and Pd with Br assistance was further investigated under varying potentials from 1.6 V_{RHE} to 2.4 V_{RHE}. Specifically, the charge required for the theoretical full conversion of substrates (150 C) was injected at different potentials during the electrolysis, and the products were quantified by Gas Chromatography (Supplementary Fig. S10). As shown in Fig. 2c–e, no obvious cyclohexene oxide was produced on the PdO electrode without bromine ions, whereas the side oxidation products at the α-position of cyclohexene, including cyclohexanone and cyclohexanol, were observed (Supplementary Fig. S11). Overall, a low level of conversion was observed in this case, confirming that the oxygen species generated on the PdO surface alone could hardly activate the C=C bond of cyclohexene[51].

In sharp contrast, the formation of epoxy compounds was clearly observed on both PdO and Pd in the presence of bromine ions. The cyclohexene oxide product was further verified by GC-MS (Supplementary Fig. S12), ^{1}H NMR, and ^{13}C NMR (Supplementary Fig. S13) characterizations. As shown in Fig. 2c, d, the optimal performance on PdO was achieved at a relatively low potential of 1.6 V_{RHE}. This significantly reduced the overpotential benefits of the practical application of electrochemical epoxidation by minimizing side reactions such as OER or the formation of other organic oxidation products. A decline in the yield and FE of cyclohexene oxide was observed with more positive potentials within the range of 1.8 to 2.4 V_{RHE}. In comparison, metal Pd exhibited a relatively lower epoxidation performance, which, on the other hand, showed a gradual increase with more oxidizing potentials. This opposite trend on Pd can be rationalized by the necessary role of the Pd oxide state in the catalytic cycle of cyclohexene epoxidation, which becomes more abundant on Pd due to its own surface oxidation (Pd→PdO_x→PdO) under higher potentials. Indeed, when the anodic potential increases to > 2 V_{RHE}, Pd exhibits similar performance to PdO as a result of a largely oxidized Pd surface. The in situ electrochemical impedance spectroscopy (EIS) was further conducted on both PdO and Pd electrodes, and the fitting results (Supplementary Fig. S14) provided more insights into the mechanistic similarity/difference between Pd and PdO during epoxidation. Specifically, with the addition of cyclohexene at low oxidation potentials (1.4 V_{RHE}), a weak increase in R_{ct} from 1043 Ω to 1181 Ω was observed in PdO, whereas Pd showed a significantly larger increase in R_{ct} from 1675 Ω to 6954 Ω, indicating the slow interfacial electron transfer (from the organic matter to electrode) on Pd. In comparison, at high oxidation potential (1.8 V_{RHE}), the R_{ct} values were generally two orders of magnitude lower, and the addition of substrate resulted in a negligible change in the R_{ct} on both PdO (from 59.3 Ω to 91.1 Ω) and Pd (from 13.3 Ω to 21.1 Ω) electrodes. This suggests that at high oxidation potentials, the Pd catalyst presumably went through an *operando* surface reconstruction and developed an oxidized surface (the active state) that was similar to PdO. Such surface oxidation process, however, did not occur under low oxidation potentials (< 1.8 V_{RHE}), thus the intrinsic low oxygenating kinetics on metallic Pd surface was observed instead. To further reveal the surface oxidation process of metal Pd at different potentials, in situ electrical transport spectroscopy (ETS) was conducted on Pd. As shown in Supplementary Fig. S15, the declining conductivity corresponding to the oxidative adsorption of OH* on the Pd surface (between 1.4 and 1.7 V_{RHE}) and subsequent surface oxidation to PdO_x (after the potential of 1.7 V_{RHE}) can be observed, demonstrating the evolution of surface oxidation states on Pd. The three dETS peaks identified at 1.4, 1.75, and 1.95 V_{RHE} can be assigned to the formation of Pd-OH*, PdO_x, and PdO, respectively. Overall, the evolution of epoxidation kinetics on Pd with varying oxidation potentials and its similar performance to PdO at a specific potential range can be rationalized by its surface oxidation as indicated by the EIS and ETS results.

https://doi.org/10.1038/s41467-024-53049-z

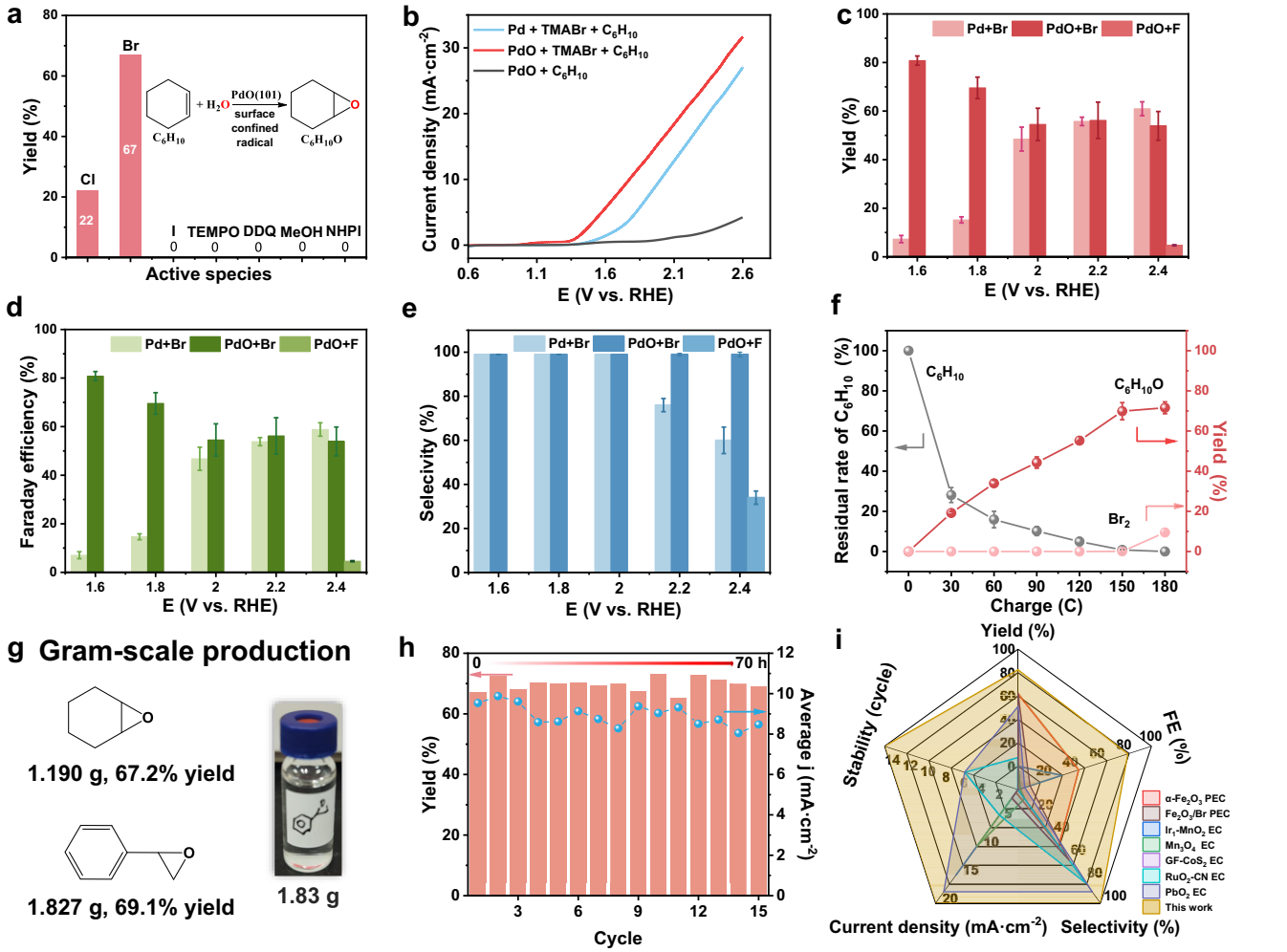

Fig. 2 | The electrocatalytic performance of radical-assisted olefin epoxidation. **a** The screening of cyclohexene epoxidation performance (epoxide yields) with different activation species, including Cl^-, Br^-, I^-, TEMPO, MeOH, DDQ, and NHPI. **b** The linear sweep voltammetry (LSV) of Pd in 0.1 M TMABr and PdO in 0.1 M TMAF or TMABr. The scan rate is 10 mV/s. **c**–**e** The reaction yields (**c**), Faraday efficiencies (**d**), and selectivity (**e**) of cyclohexene oxide production under potential, standard condition: 5 mL MeCN + 10 mL H_2O, 100 mM TMABr + 50 mM C_6H_{10}. **f** Correlation between the conversion of cyclohexene, yield of cyclohexene oxide/Br_2, and the consumed charge. Reaction condition: 0.1 M TMABr + 0.05 M C_6H_{10} in 15 mL MeCN/H_2O (volume ratio 1:2), @1.8 V_{RHE}. **g** The gram-scale production of cyclohexene and styrene oxides. Reaction condition: for cyclohexene, 36 mmol TMABr + 18 mmol cyclohexene in 60 mL MeCN/H_2O (volume ratio 1:2), @1.8 V_{RHE}, 3473 C; for styrene, 44 mmol TMABr + 22 mmol styrene in 60 mL MeCN/H_2O (volume ratio 1:2), @1.8 V_{RHE}, 4245 C. **h** Recycling performance of the PdO-Br system. After the completion of a standard reaction, the electrolyte was replaced, and a new cycle of electrolysis was initiated with the same catalyst. Blue dots are the average current density for each cycle. Reaction condition: 0.1 M TMABr + 0.05 M C_6H_{10} in 15 mL MeCN/H_2O (volume ratio 1:2), @1.8 V_{RHE}. **i** The comparison of catalytic performance metrics of cyclohexene epoxidation via surface-confined radical strategy with state-of-the-art (photo-)electrochemical methodologies, error bars in **c**–**f** represent the standard deviation from multiple reactions ($n = 3$).

Overall, the PdO-Br system ultimately achieves a record-high cyclohexene-to-cyclohexene oxide yield (82%) and Faraday efficiency (81%). More importantly, as shown in Fig. 2e, PdO-Br-catalyzed cyclohexene epoxidation achieves > 99% selectivity towards cyclohexene oxide, which is key to economical epoxy production for its industrial application. No side products or cyclohexene were detected after the reaction (Supplementary Figs. S16, S17). The loss of carbon efficiency can be attributed to the possible excessive oxidation of cyclohexene, toward carbon dioxide or polymerization on the electrode surface. Note that no significant difference in the electrochemically active surface area was observed between the PdO and Pd surface (illustrated in Supplementary Fig. S18), which excludes the possible influence of ECSA on the distinct catalytic characteristics of these two surfaces. It is also interesting to note a linear correlation between the quantity of cyclohexene oxide product and the electrical charge consumption, whereas the concentration of cyclohexene decreases exponentially (Fig. 2f). This observation suggests that the conversion of cyclohexene-to-cyclohexene oxide occurs via an intermediate form, and its oxidation is presumably the critical step.

On the basis of the exceptional performance of the PdO-Br catalyst in olefin epoxidation, the stability, and scalability of the catalytic system were also tested for practical considerations. A gram-scale reaction was first conduced, as shown in Fig. 2g, when the reaction was scaled-up to 18 mmol of cyclohexene, 12.1 mmol of cyclohexene oxide can be obtained with a yield of 67.2% (one batch). Similar scaling-up tests were additionally conducted on styrene, where 2.31 g (~ 22 mmol) of styrene was utilized to produce about 1.83 g of styrene oxide with a yield of 69.1%. The separated final products after purification were characterized by ^1H NMR,^{13}C NMR (Supplementary Fig. S19), and GC-MS (Supplementary Fig. S20). The successful realization of the gram-scale reaction demonstrates the promising potential for the application of this strategy. As shown in Fig. 2h, the PdO electrode could be utilized repeatedly for the anodic oxidation of cyclohexene, while its activity and the average current density did not exhibit any significant

decline after fifteen cycles (up to 70 hrs). The catalysts after repeating electrolysis cycles were further characterized by XRD (Supplementary Fig. S21), XPS (Supplementary Fig. S22), and SEM tests (Supplementary Fig. S23), which revealed no significant changes in the crystalline shape, electronic properties, and morphology of the catalyst. These results suggest that the system possessed satisfactory stability for the electro-oxidation of cyclohexene. To investigate the substrate scope of this PdO-Br-based epoxidation approach, a variety of types of olefins have been used as substrate molecules, as shown in Table 1. Importantly, the strategy shows universally satisfying compatibility for conjugated olefins, cyclic olefins, and chain olefins and achieves > 70% yield, selectivity, and Faraday efficiency in general.

Overall, in comparison to state-of-the-art electrochemical or photoelectrochemical (PEC) cyclic olefin oxidation reactions, the PdO-Br system developed in this work demonstrates performance with respect to conversion, yield, Faraday efficiency, selectivity, and substrate scopes (Fig. 2i and Supplementary Table 1). Note that selectivity in Fig. 2i was calculated by the molar ratio of cyclohexene·oxide over obtained organic matter adapted in these reports. Moreover, given that the up-to-date thermo-catalytic olefin oxidation approaches often included the use of oxygen or peroxide, this electrochemical strategy also offers mild reaction temperatures, no use of potentially hazardous oxygen source, and excellent reaction performance, as summarized in Supplementary Table S2.

Mechanistic study on the PdO-Br-based epoxidation of olefins

For mechanistic investigations, electrochemical titration experiments[23] were conducted to reveal the adsorption of cyclohexene on the PdO surface. First, the LSV results of cyclohexene in tetramethylammonium fluoride (TMAF) solution in Fig. 3a depict the obviously lower onset potential for the direct oxidation of cyclohexene (at approximately 1.35 V_{RHE}) as compared to the OER (onset at approximately 1.8 V_{RHE}). We then employed pulsed chronoamperometry (CA) measurement to verify the adsorption of cyclohexene molecules on the PdO electrode before the onset of cyclohexene oxidation. Specifically, the electrode was first kept at a constant potential (in the range of 1.1 V_{RHE} to 1.3 V_{RHE}) for 1 h in the presence of cyclohexene to reach an equilibrium in surface adsorption. The electrode was then transferred into the electrolyte without cyclohexene and was simultaneously set to a high oxidation potential of 1.8 V_{RHE}. As shown in Fig. 3b and Supplementary Fig. S24, an obvious surge in the anodic current (from the oxidation of surface organic molecules) was observed after the switch, confirming the adsorption of cyclohexene molecules on PdO at the low potential region. Furthermore, the amount of molecular adsorption (as indicated by the oxidation current level) appears to be positively correlated with the initial adsorption potentials. The surface adsorbed cyclohexene was further verified by the powder diffuse reflectance infrared spectroscopy (IR), the inset in Fig. 3b displays the characteristic IR peaks of the CH_2 structure. Similarly, bromine adsorption was also observed in the pulsed CA measurement (Supplementary Fig. S24), and the control experiment (without the presence of cyclohexene and Br^-) indicated no obvious surface adsorption of other species, excluding the possible influence of anionic effect and other reactions. In addition, electrolytic epoxidation of cyclohexene conducted using $H_2{}^{18}O$ confirmed the origin of the oxygen atoms from partial-water oxidation. GC-MS characterizations of the epoxide product (Fig. 3c and Supplementary Note 1) clearly indicated that water is the sole source of oxygen, and the surface olefin intermediates (after activation) presumably went through a water-assisted oxidation mechanism with a nucleophilic attack by the surface oxygen species[22,52].

The critical role of bromine-based activation on PdO subsequent to the olefin adsorption was further investigated. We first noticed that the presence of a smaller amount of bromide ions (0.01 M, 0.2 eq) also led to a similar level of yield (~ 71.15%) under standard conditions, with an obviously reduced current density, confirming its catalytic role in the reaction cycle. Different bromine-containing substances, including Br_2, BrO^-, BrO_3^-, and Br radicals (see experimental method in Supporting Information for detailed generation of each Br species), were then added to the reaction mixture for product analysis. As shown in Fig. 3d, none of these Br species led to cyclohexene epoxidation activity under standard reaction conditions, except for bromine radicals where trace amounts of cyclohexene oxide product can be detected. This result demonstrates the negligible activity of general Br species for cyclohexene epoxidation in the solution phase, and the observed high performance under Br-assisted electrocatalytic conditions was probably due to the contribution of in situ formed Br radicals during a surface process. Note that in the controlled charge electrolysis, the formation of bromine molecules (quantitatively determined by iodine titration method, see Supplementary Fig. S25)[53], only started to appear when the conversion of cyclohexene epoxide was complete (Fig. 2f). Therefore, the electrochemically formed interfacial Br radicals were proposed to be largely consumed by the surface-adsorbed cyclohexene, with negligible diffusion into the solution phase to form Br_2 via dimerization. In addition, as Br_2 molecules can readily react with cyclohexene to form a dibromo product, its absence in the final product (Supplementary Fig. S16) further supports the conclusion that bromine radicals serve as a surface-active intermediate species during the catalytic cycle. To further track intermediates during the radical pathway over PdO, electron paramagnetic resonance (EPR) was conducted with 5,5-dimethyl-1-pyrroline N-oxide (DMPO) as a trapping agent. As shown in Fig. 3e, after electrolysis at 1.8 V_{RHE} for 1.5 h under standard conditions without C_6H_{10}, three peaks at 3501.0, 3508.0, and 3515.2 G corresponding to the DMPO-Br can be observed. Meanwhile, the peaks at 3497.1, 3504.3, 3511.3, and 3519.1 G can be attributed to hydroxyl radicals (DMPO-OH)[38], suggesting that oxygen evolution reaction (OER) intermediates may also be involved in the reaction. Stronger EPR signals can be observed at higher potential (2.0 V_{RHE}). With the addition of cyclohexene, the EPR signals were weakened, which is consistent with the hypothesis that electrochemically generated bromine radicals preferentially react with adsorbed cyclohexene on the PdO surface, rather than being trapped by DMPO in solution. The radical clock experiment also verified the presence of hydroxyl and bromine radicals[54–56]. (see detailed information in Supplementary Fig. S26).

We therefore propose that the cyclohexene oxidation process can be divided into three critical steps: (1) adsorption of cyclohexene molecule on the PdO surface, (2) the C=C bond activation via surface-confined bromine radicals generated by the anodic oxidation of bromide ions, and (3) attack of the activated cyclohexene intermediate by the surface active oxygen species (from partial water oxidation) to afford the final epoxide products. On the basis of this surface-radical-oxidation mechanism, a screening process was further conducted to assess the cyclohexene oxidation performance of various commonly used OER catalysts under the same conditions. As shown in Fig. 3f and Supplementary Figs. S27, S28, the cyclohexene oxidation performance of different catalysts shows a linearly positive correlation with its ability to oxidize the bromide ions and cyclohexene (evaluated by the oxidation onset potentials[22,57–59]), in sharp contrast to the trend in OER, and the correlation is higher for simultaneous oxidation of bromide ions and cyclohexene. These results suggest that the intrinsic organic oxidation (adsorption) ability and the promotion of Br activation, rather than the generation of active surface oxygen species, are both key factors that determine the epoxidation efficiency. This observation is consistent with the proposed catalytic mechanism for the water-assisted oxidation of relatively inert organic entities.

Electrokinetic studies were conducted to further elucidate the epoxidation mechanism. A detailed theoretical micro-kinetic model was constructed, which can be found in Supplementary Note 2 and Supplementary Fig. S29. As shown in Fig. 4a, PdO exhibits a unique

https://doi.org/10.1038/s41467-024-53049-z

Table 1 | Catalytic performance with different substrates

Olefins type	Substrate	Product	Yield / %	Selectivity / %	FE / %
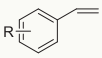 Conjugated olefins			83.5	89.8	80.5
	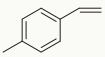	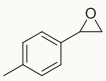	70.0	86.1	67.5
	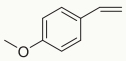	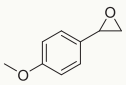	65.5	72.0	63.1
	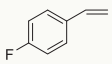	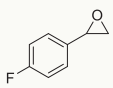	77.1	92.6	74.4
	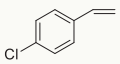	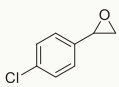	66.2	87.2	63.8
	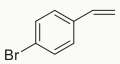	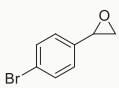	67.9	97.3	65.5
	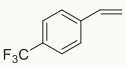	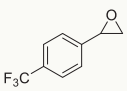	41.2	87.6	39.8
 Cyclic olefins			74.6	84.6	72.0
			70.5	100.0	68.2
			76.5	96.6	73.6
			66.4	91.8	68.5
 Chain olefins			79.6	89.6	76.8
			74.0	91.5	71.8
	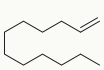	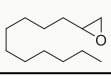	75.0	89.0	72.0

*The reaction solvent was 5 mL acetonitrile + 10 mL water, 0.1 M TMABr, and 0.05 M reaction substrate at a reaction potential of 1.8 V vs. RHE and a controlled reaction charge of 150 ~ 200 C. Quantitative analysis by GC-MS, NMR, and GC. Yield, selectivity, and Faraday efficiencies were calculated in a similar manner as for cyclohexene.

https://doi.org/10.1038/s41467-024-53049-z

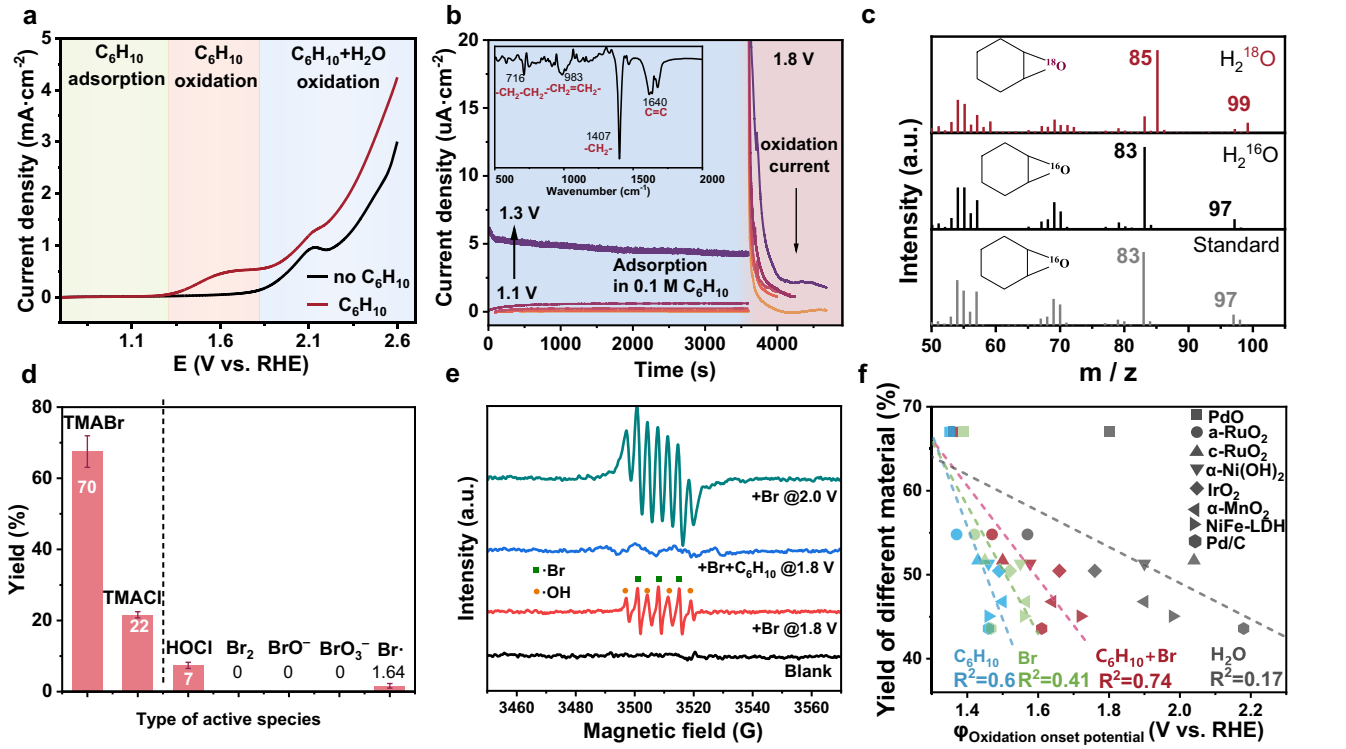

Fig. 3 | Mechanistic investigations. a The linear sweep voltammetry (LSV) of PdO in 0.1 M TMAF, the scan rate is 10 mV/s. **b** The pulsed chronoamperometry (CA) measurement where PdO electrode was first kept in 0.05 M cyclohexene (for cyclohexene adsorption) and 0.1 M TMAF at 1.1–1.3 V_{RHE} for 1 hr (highlighted by area of blue color), following by a switch of potential to 1.8 V_{RHE} and to the electrolyte of 0.1 M tetrabutylammonium perchlorate (TBAP, for cyclohexene oxidation, highlighted by area of red color); the inset is Fourier transform infrared spectroscopy (FTIR) of PdO powder, which was immersed in 0.1 M cyclohexene for 1 hour. **c** Mass spectra of cyclohexene oxide for the electro-oxidation of cyclohexene in CH_3CN-^{18}O-labeled water, CH_3CN–water, and standard theoretical isotopic distributions. **d** Systematic evaluation of possible active species (for a reaction time of 6 hours). TMABr and TMACl were reactive by forming Br·/Cl· radicals under standard electrochemical conditions. HClO, Br_2, BrO^-, and BrO_3^- were directly added as active chemical species, and free Br· radical was introduced by photochemical generation, error bars in (**d**) represent the standard deviation from multiple reactions ($n = 3$). **e** The EPR test of reactive free radical species. **f** The relationship between cyclohexene oxidation reaction performance and the onset potential values for oxidation of water, bromine ion, cyclohexene, bromine +cyclohexene, from different catalytic materials of α-MnO_2, α-$Ni(OH)_2$, amorphous-RuO_2, commercial-RuO_2, commercial-IrO_2, NiFe-LDH, Pd/C, and PdO.

current-concentration dependence that fits to the Langmuir-Hinshelwood (L-H) mechanism (also see Supplementary Table S3 for parameter fitting results), indicating a surface bimolecular reaction that presumably occurs between adsorbed cyclohexene and active bromine species. Note that as several materials exhibited close-to-zero current densities at 1.6 V_{RHE}, the current densities at 1.8 V_{RHE} were generally utilized for micro-kinetic analysis (Supplementary Fig. S30). Similar to the micro-kinetic analysis of cyclohexene, the kinetic dependence on Br^- concentrations also demonstrates a typical L-H surface bimolecular model on PdO (see Supplementary Fig. S31 and Supplementary Table S3). Surprisingly, it was observed that all other electrode materials appear to follow the Eley-Rideal (E-R) mechanism (Fig. 4b) with Тёмкин-like monotonic decreasing kinetics (see Supplementary Fig. S29b and Supplementary Table S4 for more details), in which the current densities were determined only by Br oxidation. These electro-kinetic results clearly imply a surface-confinement of Br radicals that only occurs on PdO, probably due to the enhanced adsorption and surface coverage (θ_{olefin}) of olefin molecules, which subsequently creates a spatial proximity that efficiently facilitates the bimolecular reaction kinetics between adsorbed cyclohexene and bromine radicals on the PdO surface. This surface-confined reaction pathway effectively restricts the radical activation process to the surface and avoids the general issues of insufficient conversion and unfavorable side reactions from the homogenous process. For other materials, the weak adsorption of cyclohexene (low surface binding energies) on the electrode surface leads to its negligible surface coverage, and the overall electro-kinetics are determined by the reaction between surface bromine radicals and proximate free cyclohexene molecules from the solution phase, which is presumably much slower compared to surface-confined bi-molecular reaction (as also indicated by the fitting results of rate constant k_3''', which is significantly higher in L-H pathway than in E-R pathway, see Supplementary Tables S3, S4).

Electrochemical in situ infrared spectroscopic characterizations provided additional insights into the surface adsorption of cyclohexene during the epoxidation process. As shown in Fig. 4c and Supplementary Fig. S32, starting from 1.3 V_{RHE}, the upward bands at 1637, 1373–1487, and 916–949 cm^{-1} were observed on PdO in the presence of cyclohexene, which can be assigned to the C=C, -CH_2, and -CH = CH- structure of adsorbed cyclohexene, respectively. The adsorption of cyclohexene remains largely unchanged across a wide range of electrochemical potentials (1.3–2.0 V_{RHE}), indicative of its chemical inertness under such conditions. Conversely, with the addition of bromine, the intensities of all cyclohexene peaks gradually diminished to a low level with the increasing anodic potentials, as highlighted in Fig. 4c (also see Supplementary Fig. S32c for the summary), indicating its effective conversion facilitated by bromine radicals. The overall adsorption intensity of cyclohexene also demonstrated a notable decrease following bromine addition (Supplementary Fig. S32c), suggesting competitive adsorption between bromine and cyclohexene on the PdO surface. For catalysts predominantly following the E-R mechanism, such as metal Pd, intrinsically weak adsorption of

https://doi.org/10.1038/s41467-024-53049-z

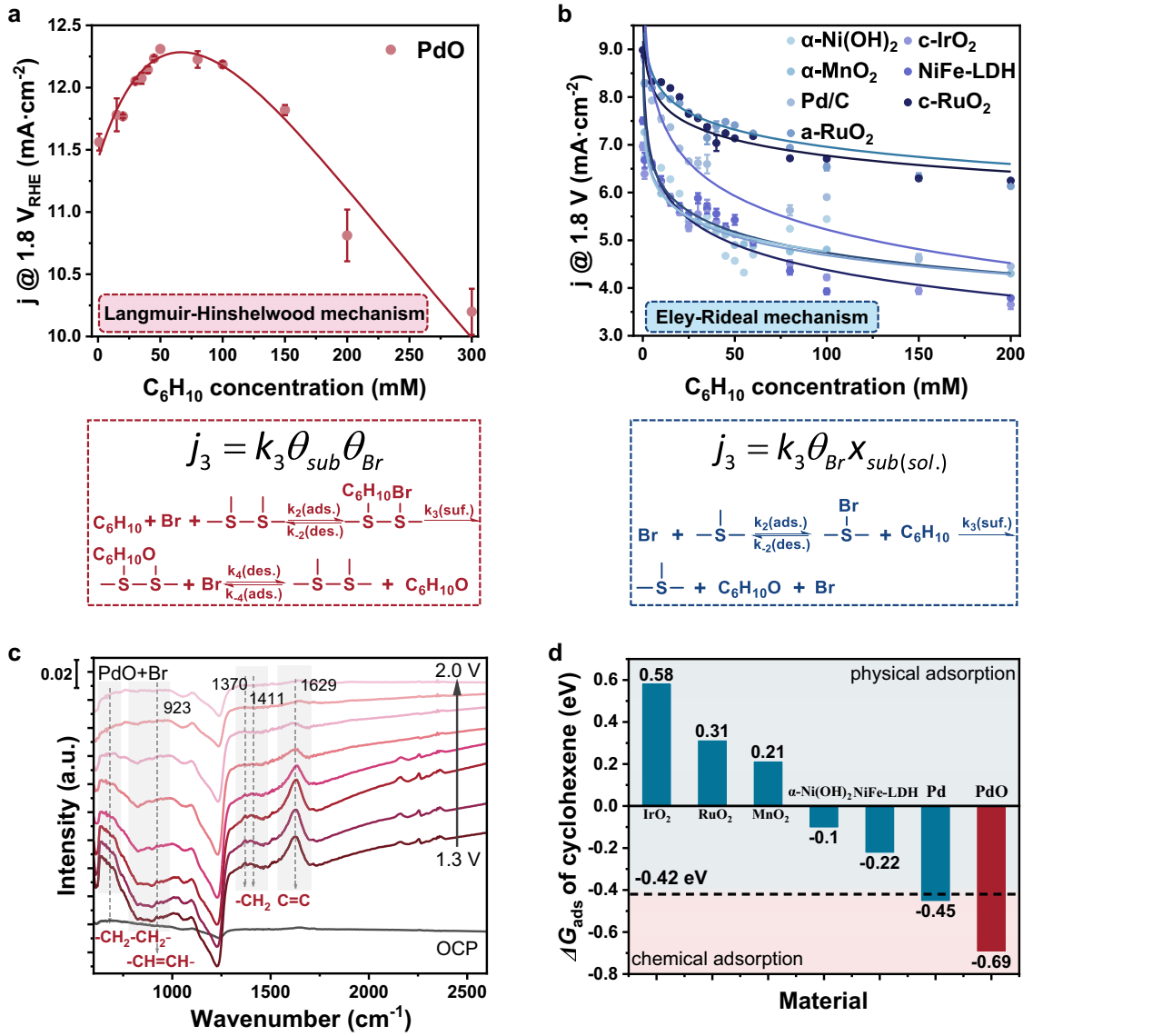

Fig. 4 | Kinetic and mechanistic investigations. a, **b** The kinetic analysis of PdO (**a**) and other seven catalysts (**b**), data points depict the dependence of experimental partial current densities (equivalent to reaction rates under high FEs) on the cyclohexene concentrations, and the solid curves show the mathematical fitting of the kinetic data. **c** Electrochemical in situ ATR-FTIR spectra of PdO vary from 1.3 V_{RHE} to 2.0 V_{RHE}, solution: 0.1 M TMABr+0.05 M C_6H_{10} in MeCN/H_2O (1:2); **d** The adsorption energy of cyclohexene with different material.

cyclohexene was first observed (e.g., substantially lower peak intensities at 1623 cm^{-1}), with negligible change under oxidizing electrochemical potentials (see Supplementary Fig. S32b). This behavior further correlates the low reactivity of cyclohexene to its weaker initial adsorption under such conditions. Note that the C=C adsorption peak slightly diminished at high potentials (> 1.8 V_{RHE}), which can be attributed to the unique surface oxidation of Pd (towards PdOx-like characteristics).

This behavior underscores the low reactivity of cyclohexene on materials following the E-R mechanism, which can be attributed to its weaker initial adsorption and inert interaction with bromine. To further rationalize the different micro-kinetic behaviors on PdO and other catalytic surfaces, the adsorption energies of cyclohexene on different materials were evaluated using DFT calculations (see calculation details in "Methods"). As shown in Fig. 4d and Supplementary Fig. S33, PdO exhibits a much more negative ΔG_{ads} for cyclohexene, in sharp contrast to other materials. It is interesting to note that ΔG_{ads} of approximately − 0.42 eV have been generally considered the boundary between physisorption (via van der Waals interaction) and chemisorption (via chemical bonding)[60,61]. Results in Fig. 4d indicate that cyclohexene undergoes distinct chemisorption on PdO, resulting in significantly enhanced surface coverage. This result further rationalizes the unique micro-kinetic behavior on PdO (bi-molecular reaction between surface adsorbed olefines and Br radicals in situ generated on electrode).

The summarized mechanism of cyclohexene electrooxidation on the PdO surface, facilitated by surface-confined bromine radical pathway, is schematically illustrated in Fig. 5a. Density functional theory (DFT) calculations were carried out to further elucidate the mechanistic pathways for both direct surface oxidation and oxidation through surface-confined radical pathways. As shown in Fig. 5b and Supplementary Fig. S34, the carbon-carbon double bond of cyclohexene is readily adsorbed to the Pd atom via a bridging configuration on PdO[40]. In a direct oxidation pathway, the adsorbed cyclohexene is directly oxidized by the lattice oxygen to produce a C-O bond. In the surface-confined radical pathway, however, the adsorbed cyclohexene is more readily coupled to the bromine radical to form an intermediate

https://doi.org/10.1038/s41467-024-53049-z

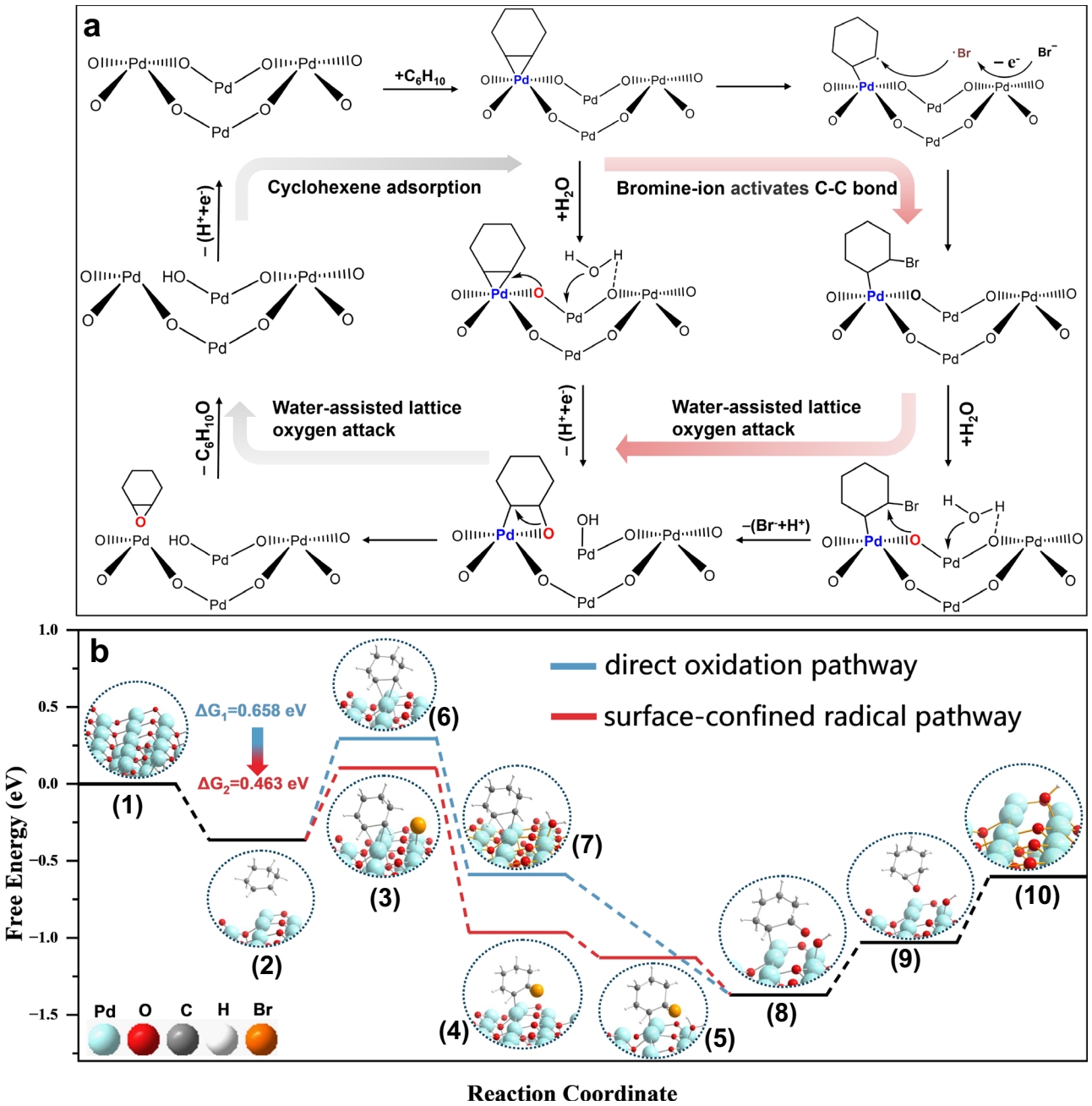

Fig. 5 | Possible mechanisms and theoretical calculations. a The possible mechanism of cyclohexene oxidation via direct oxidation pathway and bromine-ion surface-confined radical pathway. **b** Reaction-free energy diagrams for the cyclohexene epoxidation by direct oxidation pathway and surface-confined radical pathway on the PdO (101) surface.

C-Br bond, followed by its subsequent O replacement to form cyclohexane oxide. It is evident the presence of bromine radical pathway efficiently reduces the free energy of cyclohexene activation from 0.658 eV to 0.463 eV, with more smooth energy steps (presumably lower energy barriers) via (2) → (3) → (4) → (5) → (8) as compared to (2) → (6) → (7) → (8).

Discussions

Together, our studies offer a universal high-efficiency electrocatalytic olefin epoxidation approach through the combination of a kinetically controlled, surface-confined radical activation and consequent water-assisted oxidation, that achieves successful electro-epoxidation of a variety of olefin molecules with record-high performance. Over 80% yield and FE were obtained for cyclohexene epoxidation to cyclohexene oxide, concurrently with >99% product selectivity and excellent system stability. Such electrocatalytic epoxidation strategy appears effective, moreover, for a wide scope of olefins, including chain olefins (~ 70% yield), cyclic olefins (~ 80% yield), and conjugated olefins (~ 80% yield). We further show the gram-scale electrolytic epoxide production to demonstrate its potential industrial applications. Overall, this work represents another important milestone for the rational design of the "green oxygen strategy" driven by renewable energy and green, safe, and atomically-economic water oxygen source, to produce valuable chemicals via the electrooxidation of inactive organics. More importantly, it sheds light on the development of effective modulation principles for the activation and oxidation of relatively inert chemical bonds, which are key to achieving overall manufacturing sustainability.

Methods

Preparation of the epoxidation catalysts

PdO was prepared by direct Pd oxidation. The Pd/C catalysts were purchased from Adamas (10 wt% loading). Specifically, Pd/C powders were heated up to 350 °C at a rate of 5 °C/min and kept for 4 h in a muffle furnace. Subsequently, the samples were further heated up to 600 °C and kept for another 2 h. Finally, the powders were cooled naturally in ambient (or in the furnace) to room temperature to produce PdO (101) catalyst powders.

General material characterizations

XRD patterns were collected on a Bruker D8 ADVANCE X-ray diffractometer equipped with a Cu-Kα radiation source ($\lambda = 0.15418$ nm) operating at 40 kV and 40 mA. The morphology of the samples was analyzed by scanning electron microscopy (SEM, Hitachi S-4800) with samples deposited on carbon conductive tapes. The elemental analysis was conducted with field emission scanning electron microscopy (FESEM, Nova NanoSEM 450) with an additional energy dispersive spectroscope (EDS). Transmission Electron Microscopy (TEM) and High-resolution TEM images were obtained on JEOL JEM-1011 and JEM-2100, respectively, with samples deposited on carbon-coated Cu grids. X-ray photoelectron spectroscopy (XPS) was performed on a Thermo Fischer ESCALAB Xi+ with Al Kα (hv = 1486.6 eV) as the radiation source. The binding energies were calibrated by the C 1s peak, and the internal standard reference was at 284.6 eV. Raman spectra were recorded on a Horib France Sas Xplora Plus Raman spectroscopy equipped with a 532 nm laser source. Fourier Transform Infrared Spectrometer (FTIR) was recorded on Bruker Tensor 27.

Electrochemical methods

Electrochemical experiments were typically conducted in a single electrochemical cell with a standard three-electrode system controlled by a Corrtest CS3004 workstation. Catalyst powders (5 mg) were dispersed in the mixed solvent of DI water (480 μL) and ethanol (480 μL), with the addition of Nafion (5 wt% in propanol, 40 μL), to make a catalyst suspension ink. The catalyst ink was then coated on pre-treated carbon paper (CP, $1 \times 2\ cm^2$) to prepare the working electrode (0.5 mg/cm2 loading). Saturated potassium chloride (Ag/AgCl) and Pt tablet electrodes ($1 \times 1\ cm^2$) were used as reference electrodes and counter electrodes, respectively. Linear sweep voltammetry (LSV) was measured with a scan rate of 10 mV/s. In situ electrochemical impedance spectroscopy (EIS) tests were conducted over a frequency range from 10^4 to 10^{-2} Hz with an AC amplitude of 5 mV. Except for the EIS, agitation was maintained throughout all electrochemical tests. All potentials in this study were measured against the Ag/AgCl and converted to the RHE reference scale by E (V vs. RHE) = E (V vs. Ag/AgCl) + 0.0591 × pH + 0.198. All the potentials were not IR compensated.

Electrolysis section

For screening of active substances, 15 mL of electrolyte (10 mL DI water and 5 mL MeCN) containing Tetramethylammonium fluoride (TMAF, acts as electrolyte support), cyclohexene (50 mM), and active substances (100 mM) was added into the undivided cell with a micro-magnetic spin bar for stirring. Constant-potential electrolysis was used with a controlled amount of electricity at a reaction potential of and a reaction charge of 150 C. For each bulk electrolysis measurement, 15 mL of electrolyte (10 mL DI water and 5 mL MeCN) containing cyclohexene (50 mM) and Tetramethylammonium bromide (TMABr, which acts as an electrolyte and active species) was added into the undivided cell with a micro-magnetic spin bar for stirring. Constant-potential electrolysis was used with a controlled amount of electricity at a reaction potential of and a reaction charge of 150 C. After the reaction finished, the whole reactant was extracted with ethyl acetate instantly. After the internal standard benzyl chloride was added, the organic phase was sampled for GC analysis. To obtain electro-kinetic data in Fig. 2f, the chronoamperometry analysis was conducted at 1.8 V (vs. RHE) until the charge was passed for 30 ~ 180 C, dependent on the substrate concentration. To minimize errors, the same electrode is used for each type of electrochemical test.

Product analysis

Typically, three independent electrolysis experiments were parallelly conducted with each catalyst for performance evaluation. Gas chromatography (GC) measurements were conducted on a Shimadzu Nexis GC-2030 with a flame ionization detector and SH-Rtx-1 capillary column (30 m, 0.25 mm ID, 0.25 μm df). For quantitative product analysis, the sample was injected for 3 times to get a mean value for one electrolysis. The temperature of the column was initially kept at 40 °C for 1 min and first increased to 150 °C at a rate of 5 °C/min. Then the temperature was increased to 250 °C at a rate of 25 °C/min and kept for 3 min. Benzyl chloride was used as the internal standard for the quantification of the chemicals. The conversion of cyclohexene, the yields, selectivity, and Faradaic efficiency (FE) of cyclohexene oxide were calculated as follows:

$Conversion_{C6H10}$ = (1 − mol of cyclohexene / mol of loaded cyclohexene) × 100%

$Yield_{C6H10O}$ = (mol of product / mol of loaded cyclohexene) × 100%

FE_{C6H10O} = mol of cyclohexene oxide / [totally passed charge / (2 × F)] × 100%

$Selectivity_{C6H10O}$ = (mol of cyclohexene oxide / mol of obtained organic matter) × 100%

For substrate expansion experiments: Yields and Faraday efficiencies were calculated similarly to cyclohexene, but since the by-products could not be fully quantified, selectivity was calculated as follows:

$Selectivity_{epoxides}$ = (yield of epoxides / conversion of olefins) × 100%

Electrochemical in situ ATR-FTIR tests

Electrochemical in situ ATR-FTIR measurements were performed on a Bruker INVENIOS instrument mounted with an ATR liquid phase cell and an MCT detector. The reaction solution was the same as in the electrolysis experiments, and the IR signals were collected after 20 min of electrolysis at each potential.

Computational details

We have employed the first principles to perform spin-polarization density functional theory (DFT) calculations by using the Vienna ab initio simulation package (VASP 5.4.1) within the generalized gradient approximation (GGA) using the Perdew-Burke-Ernzerhof (PBE) formulation. We have chosen the projected augmented wave (PAW) potentials to describe the ionic cores and take valence electrons into account using a plane wave basis set with a kinetic energy cutoff of 450 eV. Partial occupancies of the Kohn–Sham orbitals were allowed using the Gaussian smearing method and a width of 0.05 eV. The electronic energy was considered self-consistent when the energy change was smaller than 10^{-5} eV. A geometry optimization was considered convergent when the energy change was smaller than 0.05 eV $Å^{-1}$. The vacuum spacing in a direction perpendicular to the plane of the structure is 16 Å. The Brillouin zone integration is performed using $2 \times 2 \times 1$ Monkhorst-Pack k-point sampling for a structure. Finally, the adsorption energies(Eads) were calculated as Eads= Ead/sub -Ead -Esub, where Ead/sub, Ead, and Esub are the total energies of the optimized adsorbate/substrate system, the adsorbate in the structure, and the clean substrate, respectively. The free energy was calculated using the equation: G = E + ZPE-TS, where G, E, ZPE, and TS are the free energy, total energy from DFT calculations, zero point energy, and entropic contributions, respectively. In our calculation, the top two layers had been relaxed, and the other layers were fixed in surface structures. For the amorphous structure, we obtain a stable amorphous structure at 300 K with ab initio first principles methods.

Data availability

The authors declare that the data supporting the conclusions of this study are available within the paper and its Supplementary Materials. The source data of graphs in the main article are provided in this paper. Additional data are available from the corresponding authors upon request. Source data are provided in this paper.

References

1. McGarrigle, E. M. & Gilheany, D. G. Chromium- and manganese-salen promoted epoxidation of alkenes. *Chem. Rev.* **105**, 1563–1602 (2005).
2. Lane, B. S. & Burgess, K. Metal-catalyzed epoxidations of alkenes with hydrogen peroxide. *Chem. Rev.* **103**, 2457–2473 (2003).
3. Yoon, T. U. et al. Cyclohexene epoxidation with H(2)O(2)in the vapor and liquid phases over a vanadium-based metal-organic framework. *Catal. Sci. Technol.* **10**, 4580–4585 (2020).
4. Wilbers, D. et al. Controlling product selectivity with nanoparticle composition in tandem chemo-biocatalytic styrene oxidation. *Green. Chem.* **23**, 4170–4180 (2021).
5. Nijhuis, T. A., Makkee, M., Moulijn, J. A. & Weckhuysen, B. M. The production of propene oxide: Catalytic processes and recent developments. *Ind. Eng. Chem. Res.* **45**, 3447–3459 (2006).
6. Gordon, C. P. et al. Efficient epoxidation over dinuclear sites in titanium silicalite-1. *Nature* **586**, 708–713 (2020).
7. Chi, M. F. et al. Spatial decoupling of bromide-mediated process boosts propylene oxide electrosynthesis. *Nat. Commun.* **15**, 3646 (2024).
8. Khatib, S. J. & Oyama, S. T. Direct oxidation of propylene to propylene oxide with molecular oxygen: A review. *Catal. Rev.* **57**, 306–344 (2015).
9. Langhendries, G., De Vos, D. E., Baron, G. V. & Jacobs, P. A. Quantitative sorption experiments on Ti-zeolites and relation with alpha-olefin oxidation by H2O2. *J. Catal.* **187**, 453–463 (1999).
10. Goetz, M. K., Bender, M. T. & Choi, K. S. Predictive control of selective secondary alcohol oxidation of glycerol on NiOOH. *Nat. Commun.* **13**, 5848 (2022).
11. Buker, J. et al. Synthesis of Cu single atoms supported on mesoporous graphitic carbon nitride and their application in liquid-phase aerobic oxidation of cyclohexene. *Acs Catal.* **11**, 7863–7875 (2021).
12. Zhong, W. Z. et al. Synergistic hollow CoMo oxide dual catalysis for tandem oxygen transfer: Preferred aerobic epoxidation of cyclohexene to 1,2-epoxycyclohexane. *Appl. Catal. B Environ.* **225**, 180–196 (2018).
13. Leow, W. R. et al. Chloride-mediated selective electrosynthesis of ethylene and propylene oxides at high current density. *Science* **368**, 1228–1233 (2020).
14. Banerjee, D. et al. Convenient and mild epoxidation of alkenes using heterogeneous cobalt oxide catalysts. *Angew. Chem. Int. Ed.* **53**, 4359–4363 (2014).
15. Engelmann, X. et al. Trapping of a highly reactive oxoiron(IV) complex in the catalytic epoxidation of olefins by hydrogen peroxide. *Angew. Chem. Int. Ed.* **58**, 4012–4016 (2019).
16. Liu, H. et al. Modulating charges of dual sites in multivariate metal-organic frameworks for boosting selective aerobic epoxidation of alkenes. *J. Am. Chem. Soc.* **145**, 11085–11096 (2023).
17. Jin, H. et al. Regulating the electronic structure through charge redistribution in dense single-atom catalysts for enhanced alkene epoxidation. *Nat. Commun.* **14**, 2494 (2023).
18. Ho, K. P., Wong, K. Y. & Chan, T. H. Indirect catalytic epoxidation with hydrogen peroxide electrogenerated in ionic liquids. *Tetrahedron* **62**, 6650–6658 (2006).
19. Zhang, Y. et al. Bromine and oxygen redox species mediated highly selective electro-epoxidation of styrene. *Org. Chem. Front.* **9**, 436–444 (2022).
20. Li, H., Abraham, C. S., Anand, M., Cao, A. & Norskov, J. K. Opportunities and Challenges in Electrolytic Propylene Epoxidation. *J. Phys. Chem. Lett.* **13**, 2057–2063 (2022).
21. Li, Y. H. et al. Redox-mediated electrosynthesis of ethylene oxide from CO2 and water. *Nat. Catal.* **5**, 185–192 (2022).
22. Sun, Y. X. et al. Highly selective electrocatalytic oxidation of amines to nitriles assisted by water oxidation on metal-doped alpha-Ni(OH)(2). *J. Am. Chem. Soc.* **144**, 15185–15192 (2022).
23. Li, Z. et al. Electrocatalytic synthesis of adipic acid coupled with H(2) production enhanced by a ligand modification strategy. *Nat. Commun.* **13**, 5009 (2022).
24. Chung, M., Jin, K., Zeng, J. S., Ton, T. N. & Manthiram, K. Tuning single-atom dopants on manganese oxide for selective electrocatalytic cyclooctene epoxidation. *J. Am. Chem. Soc.* **144**, 17416–17422 (2022).
25. Jin, K. et al. Epoxidation of cyclooctene using water as the oxygen atom source at manganese oxide electrocatalysts. *J. Am. Chem. Soc.* **141**, 6413–6418 (2019).
26. Lin, X. et al. Direct oxygen transfer from H2O to cyclooctene over electron-rich RuO2 nanocrystals for epoxidation and hydrogen evolution. *Angew. Chem. Int. Ed.* **61**, e202207108 (2022).
27. Dorchies, F. et al. Controlling the hydrophilicity of the electrochemical interface to modulate the oxygen-atom transfer in electrocatalytic epoxidation reactions. *J. Am. Chem. Soc.* **144**, 22734–22746 (2022).
28. Kato, S., Iwase, K., Harada, T., Nakanishi, S. & Kamiya, K. Aqueous electrochemical partial oxidation of gaseous ethylbenzene by a ru-modified covalent triazine framework. *Acs Appl. Mater. Inter.* **12**, 29376–29382 (2020).
29. Fan, L. et al. Selective production of ethylene glycol at high rate via cascade catalysis. *Nat. Catal.* **6**, 585–595 (2023).
30. Zhao, Y. K. et al. alpha-Fe2O3 as a versatile and efficient oxygen atom transfer catalyst in combination with H2O as the oxygen source. *Nat. Catal.* **4**, 684–691 (2021).
31. Gao, Y. et al. Membrane-Free Electrosynthesis of Epichlorohydrins Mediated by Bromine Radicals over Nanotips. *J. Am. Chem. Soc.* **146**, 714–722 (2024).
32. Jirkovsky, J. S., Busch, M., Ahlberg, E., Panas, I. & Krtil, P. Switching on the electrocatalytic ethene epoxidation on nanocrystalline RuO2. *J. Am. Chem. Soc.* **133**, 5882–5892 (2011).
33. Luo, X. et al. Benzoic acid: Electrode-regenerated molecular catalyst to boost cycloolefin epoxidation. *J. Am. Chem. Soc.* **145**, 20665–20671 (2023).
34. Zhao, Y. et al. Br(-)/BrO(-)-mediated highly efficient photoelectrochemical epoxidation of alkenes on alpha-Fe(2)O(3). *Nat. Commun.* **14**, 1943 (2023).
35. Chung, M., Jin, K., Zeng, J. S. & Manthiram, K. Mechanism of chlorine-mediated electrochemical Ethylene oxidation in saline water. *Acs Catal.* **10**, 14015–14023 (2020).
36. Liu, X. et al. Bromide-mediated photoelectrochemical epoxidation of alkenes using water as an oxygen source with conversion efficiency and selectivity up to 100. *J. Am. Chem. Soc.* **144**, 19770–19777 (2022).
37. Wang, Q. H. et al. Electrocatalytic CO upgrading to triethanolamine by bromine-assisted CH oxidation. *Angew Chem. Int. Ed.* **62**, https://doi.org/10.1002/anie.202212733 (2023).
38. Xue, W. J. et al. Bromine-enhanced generation and epoxidation of ethylene in tandem CO electrolysis toward ethylene oxide. *Angew. Chem. Int. Ed.* **62**, e202311570 (2023).
39. Gao, Y. et al. Field-induced reagent concentration and sulfur adsorption enable efficient electrocatalytic semihydrogenation of alkynes. *Sci. Adv.* **8**, eabm9477 (2022).
40. Liu, X. C. et al. Reaction mechanism and selectivity tuning of propene oxidation at the electrochemical interface. *J. Am. Chem. Soc.* **144**, 20895–20902 (2022).

41. Lum, Y. et al. Tuning OH binding energy enables selective electrochemical oxidation of ethylene to ethylene glycol. *Nat. Catal.* **3**, 14–22 (2020).
42. Chung, M. et al. Direct propylene epoxidation via water activation over Pd-Pt electrocatalysts. *Science* **383**, 49–55 (2024).
43. Bardhan, R., Zarick, H. F., Schwartzberg, A. & Pint, C. L. Size-dependent phononic properties of PdO nanocrystals probed by nanoscale optical thermometry. *J. Phys. Chem. C* **117**, 21558–21568 (2013).
44. Hoque, M. A. et al. Electrochemical PINOylation of methylarenes: Improving the scope and utility of benzylic oxidation through mediated electrolysis. *J. Am. Chem. Soc.* **144**, 15295–15302 (2022).
45. Rafiee, M., Miles, K. C. & Stahl, S. S. Electrocatalytic alcohol oxidation with TEMPO and bicyclic nitroxyl derivatives: Driving force trumps steric effects. *J. Am. Chem. Soc.* **137**, 14751–14757 (2015).
46. Reid, L. M., Li, T. F., Cao, Y. & Berlinguette, C. P. Organic chemistry at anodes and photoanodes. *Sustain Energ. Fuels* **2**, 1905–1927 (2018).
47. Fu, Z.-H. et al. Scalable selective electrochemical oxidation of sulfides to sulfoxides. *Green. Chem.* **24**, 4772–4777 (2022).
48. Horn, E. J. et al. Scalable and sustainable electrochemical allylic C-H oxidation. *Nature* **533**, 77–81 (2016).
49. Hruszkewycz, D. P., Miles, K. C., Thiel, O. R. & Stahl, S. S. Co/NHPI-mediated aerobic oxygenation of benzylic C-H bonds in pharmaceutically relevant molecules. *Chem. Sci.* **8**, 1282–1287 (2017).
50. Utley, J. H. P. & Rozenberg, G. G. Electroorganic reactions. Part 57. DDQ mediated anodic oxidation of 2-methyl- and 2-benzylnaphthalenes. *J. Appl. Electrochem.* **33**, 525–532 (2003).
51. Noh, H. et al. An Exceptionally stable metal-organic framework supported molybdenum(VI) oxide catalyst for cyclohexene epoxidation. *J. Am. Chem. Soc.* **138**, 14720–14726 (2016).
52. Sun, Y. X. et al. Highly selective electrocatalytic oxidation of benzyl C-H using water as safe and sustainable oxygen source. *Green. Chem.* **22**, 7543–7551 (2020).
53. Zhang, Y., Zhang, Y. Y. & Lin, Y. P. Fast detection of lead dioxide (PbO2) in chlorinated drinking water by a two-stage iodometric method. *Environ. Sci. Technol.* **44**, 1347–1352 (2010).
54. Omura, K. et al. A P450 harboring manganese protoporphyrin IX generates a manganese analogue of compound I by activating dioxygen. *Acs Catal.* **12**, 11108–11117 (2022).
55. Miao, W. J. et al. Iron-catalyzed difluoromethylation of arylzincs with difluoromethyl 2-pyridyl sulfone. *J. Am. Chem. Soc.* **140**, 880–883 (2018).
56. Liu, S. Z. et al. 1,2-Amino oxygenation of alkenes with hydrogen evolution reaction. *Nat. Commun.* **13**, 4430 (2022).
57. Han, S. H. et al. Ultralow overpotential nitrate reduction to ammonia via a three-step relay mechanism. *Nat. Catal.* **6**, 402–414 (2023).
58. Maayan, G., Gluz, N. & Christou, G. A bioinspired soluble manganese cluster as a water oxidation electrocatalyst with low overpotential. *Nat. Catal.* **1**, 48–54 (2018).
59. Yuan, X., Lee, K., Eisenberg, J. B., Schmidt, J. R. & Choi, K. S. Selective deoxygenation of biomass-derived carbonyl compounds on Zn via electrochemical Clemmensen reduction. *Nat. Catal.* **7**, 43–54 (2024).
60. Gautier, S., Steinmann, S. N., Michel, C., Fleurat-Lessard, P. & Sautet, P. Molecular adsorption at Pt(111). How accurate are DFT functionals? *Phys. Chem. Chem. Phys.* **17**, 28921–28930 (2015).
61. Kokalj, A. Corrosion inhibitors: physisorbed or chemisorbed? *Corrosion Science* **196**,109939 (2022).

Acknowledgements

P.R., A.Q., T.L., F.W., B.T., B.X., J.L., Y.L., and M.D. acknowledge the support by the Natural Science Foundation of China (22172075), the Natural Science Foundation of Jiangsu Province (BK20220765), and the Fundamental Research Funds for the Central Universities (020514380323, 020514380337, 020514380291 and 020514380314).

Author contributions

M.D. supervised the research. M.D. and P.R. designed the research. P.R. conducted the electrochemical testing and mechanistic studies. A.Q. carried out the separation of organic substances as well as quantitative detection. T.L. conducted the ETS measurement. F.W., B.X., J.L., and Y.L. participated in catalysts synthesis and characterization. P.R., B.T., and M.D. analyzed the data. P.R. and M.D. co-wrote the paper. All authors have given approval to the final version of the manuscript.

Competing interests

The authors declare no competing interests.

Additional information

Supplementary information The online version contains supplementary material available at https://doi.org/10.1038/s41467-024-53049-z.

Correspondence and requests for materials should be addressed to Mengning Ding.

Peer review information *Nature Communications* thanks Lei Wang and the other anonymous reviewer(s) for their contribution to the peer review of this work. A peer review file is available.